



Citation for published version:

Shen, J, Shahid, S, Amura, I, Sarihan, A, Tian, M & Emanuelsson, EAC 2018, 'Enhanced adsorption of cationic and anionic dyes from aqueous solutions by polyacid doped polyaniline', *Synthetic Metals*, vol. 245, pp. 151-159. <https://doi.org/10.1016/j.synthmet.2018.08.015>

DOI:

[10.1016/j.synthmet.2018.08.015](https://doi.org/10.1016/j.synthmet.2018.08.015)

Publication date:

2018

Document Version

Peer reviewed version

[Link to publication](#)

Publisher Rights

CC BY-NC-ND

University of Bath

General rights

Copyright and moral rights for the publications made accessible in the public portal are retained by the authors and/or other copyright owners and it is a condition of accessing publications that users recognise and abide by the legal requirements associated with these rights.

Take down policy

If you believe that this document breaches copyright please contact us providing details, and we will remove access to the work immediately and investigate your claim.

1
2 *Enhanced Adsorption of Cationic and Anionic Dyes from Aqueous*
3 *Solutions by Polyacid Doped Polyaniline*
4

5
6 Junjie Shen^{1,2*}, Salman Shahid^{1,2}, Ida Amura^{1,2}, Adem Sarihan^{1,2,3}, Mi Tian^{1,2}, Emma AC
7 Emanuelsson^{2*}

8
9 ¹Centre for Advanced Separations Engineering, University of Bath, Bath, United Kingdom,
10 BA2 7AY.

11 ²Department of Chemical Engineering, University of Bath, Bath, United Kingdom, BA2
12 7AY.

13 ³Higher Vocational School, Bilecik Seyh Edebali University, Bilecik, 11210, Turkey
14
15

16
17 Resubmitted to

18
19 Synthetic Metals

20
21 August, 2018
22
23
24
25
26
27
28
29
30
31
32
33

34
35 *Corresponding authors: J.Shen@bath.ac.uk; E.A.Emanuelsson-Patterson@bath.ac.uk

36 **Abstract**

37 A new high surface area polyaniline (PANI) adsorbent was synthesized by matrix
38 polymerization of aniline in the presence of a polyacid, poly(2-acrylamido-2-methyl-1-
39 propanesulfonic acid) (PAMPSA). Morphological and physicochemical properties of PANI-
40 PAMPSA were characterized by field emission scanning electron microscope (FESEM), Fourier
41 transform infrared spectroscopy (FTIR), X-ray powder diffraction (XRD), nitrogen
42 adsorption/desorption and zeta potential measurement. Adsorption properties were evaluated using
43 Methylene Blue (MB) and Rose Bengal (RB) as model dyes.

44 The results showed that PANI-PAMPSA obtained a well-defined porous structure with a
45 specific surface area ($126 \text{ m}^2 \text{ g}^{-1}$) over 10 times larger than that of the emeraldine base PANI
46 (PANI-EB) ($12 \text{ m}^2 \text{ g}^{-1}$). The maximum adsorption capacities were 466.5 mg g^{-1} for MB and 440.0
47 mg g^{-1} for RB, higher than any other PANI-based materials reported in the literature. The FTIR
48 analysis and zeta potential measurement revealed that the adsorption mechanisms involved π - π
49 interaction and electrostatic interaction. The adsorption kinetics were best described by a pseudo-
50 second-order model, and the adsorption isotherms followed the Langmuir model. The
51 thermodynamic study indicated that the adsorption was a spontaneous endothermic process.
52 Overall, the convenient synthesis and the high adsorption capacity make PANI-PAMPSA a
53 promising adsorbent material for dye removal.

54

55 **Key words:** polyaniline, dye adsorption, polyacid, doping, Methylene Blue, Rose Bengal

56

57 **Abbreviations:** PANI, polyaniline; PAMPSA, poly(2-acrylamido-2-methyl-1-propanesulfonic
58 acid; MB, Methylene Blue; RB, Rose Bengal; CV, Crystal Violet; MO, Methyl Orange; PR,
59 Procion Red; OG, Orange G; CBB, Coomassie Brilliant Blue; RBBR, Remazol Brilliant Blue R;
60 AG, Alizarine Cyanine Green; MG, Malachite Green; CR, Congo Red; TMP, tin (II)
61 molybdophosphate; ZSP, zirconium (IV) silicophosphate; PTSA, *p*-toluenesulfonic acid; CSA,
62 camphorsulfonic acid.

63

64 **1. Introduction**

65 Synthetic organic dyes from wastewater of textile, paper, plastic, cosmetics,
66 pharmaceutical and food industries are a major source of environmental contamination [1, 2]. It is
67 estimated that 5000 tons of dyes are discharged into the environment every year [3]. These dyes
68 impart color to water which not only damages the aesthetic nature of water, but also interferes with
69 the transmission of sunlight and thus disturbs the biological metabolism processes of aquatic
70 communities [4, 5]. More importantly, most of the dyes have serious harmful effects on human
71 beings, which span from skin and eye irritation to dysfunction of brain, liver, kidney and
72 reproductive system [1]. Due to the low biodegradability of dyes, the conventional biological
73 methods are not effective in treating dye effluents [1]. A wide range of physicochemical techniques
74 have been employed to remove dyes, such as adsorption [2], coagulation [6], membrane filtration
75 [7], oxidation [8], electrochemical destruction [9] and photochemical degradation [10]. Among
76 these techniques, adsorption has attracted great attention because of its easy operation, low cost,
77 and high efficiency [1]. Numerous types of adsorbents, such as activated carbon, zeolite, alumina,
78 silica, biomaterials, and polymers have been extensively used for dye removal [2, 11].

79 Polyaniline (PANI) is one of the most studied conducting polymers due to its ease of
80 synthesis, low cost, environmental stability and the unique doping/dedoping property [12]. The
81 emeraldine base PANI (PANI-EB) and the emeraldine salt PANI (PANI-ES) can be efficiently
82 switched to each other by doping (protonation) and dedoping (deprotonation), respectively [13,
83 14]. The utilization of PANI as potential adsorbent for dye removal is due to two reasons: (1) its
84 large amount of amine and imine functional groups are expected to interact with organic
85 compounds [12]; (2) the charge transfer induced by doping enables PANI to interact with ionic
86 species via electrostatic interaction [15]. There are several excellent reviews in the literature
87 discussing the applications of PANI-based materials for the removal of dyes from
88 wastewater/aqueous solutions, and the reader is referred in particular to those by Zare and
89 coworkers [16], and Huang and coworkers [12]. A selective summary of adsorption capacities of
90 PANI-based materials is provided in Table 1. Although PANI is widely used for dye removal,
91 there are two main challenges restricting its actual performance. Firstly, the bare PANI-EB
92 particles can easily aggregate because of the inter- and intramolecular interactions, which
93 significantly reduces the surface area and hence results in lower adsorption capacities [12].
94 Secondly, PANI doped by small molecule acid is prone to dedoping because the small molecule

95 acid evaporates easily at room temperature [17, 18], which will reduce the surface charge of PANI
 96 and therefore affect the electrostatic interaction between PANI and dye.

97

98 Table 1: A selective summary of adsorption capacities of PANI-based materials for dye removal

Material	Dye	Maximum adsorption capacity (mg g ⁻¹)	Reference
PANI-EB			
PANI nanoparticle	MB	6.1	[19]
PANI nanotube	MB	9.2	[20]
PANI nanotube/silica composite	MB	10.3	[21]
Nanostructured crosslinked PANI	MB	13.8	[22]
Nanoporous hypercrosslinked PANI	CV, MO	245, 220	[23]
PANI-ES			
PANI-HCl	PR	18.4	[15]
PANI-HCl	MO	154.6	[24]
PANI-HCl	MB	192.3	[25]
PANI-HCl	OG, CBB, RBBR, AG	175, 129, 100, 56	[26]
PANI-HCl/chitosan composite	OG, CBB, RBBR	322, 357, 303	[27]
PANI-HCl/TMP nanocomposite	MG	78.9	[28]
PANI-HCl/ZSP nanocomposite	MB	12	[29]
PANI-H ₂ SO ₄	MO	75.9	[30]
PANI-phytic acid hydrogel	MB	71.2	[31]
PANI-PTSA	OG, CBB, RBBR, AG	342, 207, 171, 95	[32]
PANI-CSA	OG, CBB, RBBR, AG	400, 231, 254, 151	[32]
PANI-CSA/polyamide 6 composite	MO	81.9	[33]
PANI-PAMPSA	MB, RB	466.5, 440.0	This study

99

100 The present work aims to overcome these challenges by doping PANI with a polyacid,
 101 namely poly(2-acrylamido-2-methyl-1-propanesulfonic acid) (PAMPSA). PAMPSA is a strong
 102 polyacid distinguished by flexible polymer backbone and short distances between sulfonic groups

103 of neighbouring repeat units [34]. PAMPSA offers many advantages compared to small molecule
104 acids: (1) PAMPSA can easily adapt its conformation to match the spatial distribution of nitrogen
105 sites in PANI and form a double-strand structure [34, 35]. The double-strand structure confers a
106 higher stability than the single-strand structure formed between small molecule acid and PANI
107 [36]; (2) PAMPSA is not volatile and will not cause dedoping; (3) PAMPSA brings large amount
108 of sulfonic, carbonyl and amide functional groups into PANI, which may improve the
109 processability and create more adsorption sites. Our previous research found that PAMPSA as a
110 dopant can improve the porosity and chemical stability of PANI membranes for organic solvent
111 nanofiltration [37]. However, to the best of our knowledge, there has been no study about
112 PAMPSA doped PANI (PANI-PAMPSA), or any polyacid doped PANI, as adsorbents for dye
113 removal.

114 Hence, the objective of the present work was to investigate the adsorption properties of
115 PANI-PAMPSA towards a cationic dye (Methylene Blue, MB) and an anionic dye (Rose Bengal,
116 RB). The experimental variables affecting optimal adsorption were evaluated. The kinetics,
117 isotherms, thermodynamics, and mechanisms of adsorption were elucidated in detail.

118

119 **2. Materials and Methods**

120 **2.1. Chemicals**

121 Analytical grade MB, RB, aniline, ammonium persulfate (APS), hydrochloric acid (HCl),
122 N-methyl-2-pyrrolidone (NMP), 4-methyl piperidine (4MP) were obtained from Sigma-Aldrich,
123 UK. The structure and chemical properties of MB and RB are summarized in Table S1. Poly(2-
124 acrylamido-2-methyl-1-propanesulfonic acid) (PAMPSA, MW 800000 g mol⁻¹) was supplied by
125 Fisher Scientific, UK. The non-woven polyethylene/polypropylene support layer (Novatexx 2431,
126 140 μm) was supplied by Freudenberg Filter, Germany. Deionized (DI) water was produced by an
127 ELGA deionizer from PURELAB Option, USA.

128 **2.2. Synthesis**

129 PANI-PAMPSA was synthesized by matrix (template) polymerization. This approach uses
130 polyacid as a template to promote the ‘head-to-tail’ coupling of aniline along the chain of the
131 polyacid macromolecule, leading to the formation of a well-defined molecular structure of PANI

132 [38-40]. Specifically, 18.23 mL (0.2 mole) of aniline, at 4:1 monomer to acid repeat unit molar
133 ratio, was dissolved in 200 mL of 0.1 M PAMPSA solution. The polymerization of aniline was
134 initiated by the slow addition of 128 mL of 1.56 M APS solution using a peristaltic pump at a
135 speed of 20 mL h⁻¹ at 15 °C. The mixture was left for 24 h under stirring for full polymerization.
136 The final solution was filtered and the obtained PANI-PAMPSA was rinsed with DI water to
137 remove unreacted chemicals, and then washed with acetone to remove oligomers. To prepare
138 PANI-EB, 18.23 mL (0.2 mole) of aniline was dissolved in 200 mL of 1 M HCl solution. The
139 polymerization process was similar to PANI-PAMPSA, but the powder obtained was stirred in
140 33.3% (w/v) ammonia solution for 4 h to deprotonate the emeraldine salt. The obtained PANI-EB
141 was then rinsed with DI water to remove excess ammonia and then washed with acetone to remove
142 oligomers. Both PANI-PAMPSA and PANI-EB were dried in a vacuum oven at 60 °C for 24 h,
143 and then ground using mortar and pestle. The final color of PANI-PAMPSA was dark green, and
144 the final color of PANI-EB was purple bronze.

145 **2.3. Characterization**

146 The morphological and physiochemical properties of PANI-PAMPSA were characterized
147 in comparison to PANI-EB. Morphology of the samples was studied by a JEOL 6301F field
148 emission scanning electron microscope (FESEM). Fourier transform infrared (FTIR) spectra were
149 obtained by a PerkinElmer Spectrum 100 ATR-FTIR spectrometer. Each FTIR spectrum had 32
150 scans with 4 cm⁻¹ resolution. The X-ray powder diffraction (XRD) patterns were obtained with a
151 Bruker AXS D8 Advance X-ray diffractometer, equipped with a Vantec-1 detector using Cu K α
152 radiation source ($\lambda = 1.5418 \text{ \AA}$). The specific surface areas were obtained from low pressure (up
153 to 1 bar) nitrogen sorption measurements at 77 K using a Micromeritics 3Flex volumetric gas
154 sorption analysis system. The specific surface area was calculated according to the British
155 Standard guidelines for the BET method [41] from regression analysis of data in the relative
156 pressure range from 0.05 to 0.3, using the manufacturer-recommended equilibration period,
157 equating to a 2 min soak time. The surface charge was determined by the zeta potential
158 measurement. Specifically, 10 mg of PANI-EB or PANI-PAMPSA was added in 20 mL of DI
159 water to make a 0.5 g L⁻¹ dispersion. The pH of the dispersion was varied between 3 and 12 by
160 the addition of 1 mM HCl or 1 mM NaOH solution. The zeta potential of the dispersion was
161 measured by a Malvern Nano ZS ZetaSizer with folded capillary zeta cells (DTS1070).

162 2.4. Dye adsorption experiments

163 The adsorption of dyes onto PANI adsorbents were carried out in batch adsorption
164 experiments. Typically, a certain amount of PANI-EB or PANI-PAMPSA was added into 20 mL
165 of dye solution at 25 °C and 300 rpm stirring condition. At regular intervals, 1 mL of the suspension
166 was withdrawn and centrifugated at 4000 rpm by a Thermo Scientific Medifuge centrifuge, and
167 the concentration of respective dye in the supernatant was measured by a Agilent Cary 100 UV-
168 Vis spectrophotometer. The concentrations of RB and MB were calibrated by Beer-Lambert law
169 at λ_{\max} values of 549 and 663 nm, respectively.

170 The experimental variables affecting adsorption, including contact time, adsorbent dosage,
171 initial dye concentration and solution pH, were evaluated. To determine the effect of adsorbent
172 dosage as well as the initial dye concentration, a series of experiments were carried out by varying
173 the adsorbent dosage from 0.1 to 0.8 g L⁻¹, and the initial dye concentration from 25 to 200 mg
174 L⁻¹. To investigate the influence of solution pH on adsorption capacity, the pH of the dye solution
175 was adjusted from 3 to 12 before adsorption, by using 1 mM HCl or 1 mM NaOH solution. The
176 adsorption kinetic, isotherm, and thermodynamic parameters were determined to characterize the
177 adsorption process. For the adsorption kinetic, isotherm and thermodynamic experiments, the
178 solution pH was fixed at pH = 7 and the adsorbent dosage was 0.5 g L⁻¹. After the adsorption
179 reached equilibrium, the dye-loaded adsorbents were separated by centrifugation, washed with DI
180 water, and dried at 80 °C for 24 h. Possible adsorption mechanisms was investigated by FTIR
181 analysis.

182 All of the experiments were done in triplicate and the average values of the results were
183 used for data analysis. The adsorption capacity and the percentage removal were calculated using
184 Eq. (1) and Eq. (2) where q_t is the adsorbed amount of dye at time t (mg g⁻¹); c_0 and c_t are the
185 initial and present dye concentrations (mg L⁻¹); V is the solution volume (L); and m is the mass of
186 PANI (g).

$$187 \quad q_t = \frac{(c_0 - c_t)V}{m} \quad (1)$$

$$189 \quad \text{Removal} = \frac{c_0 - c_t}{c_0} \times 100\% \quad (2)$$

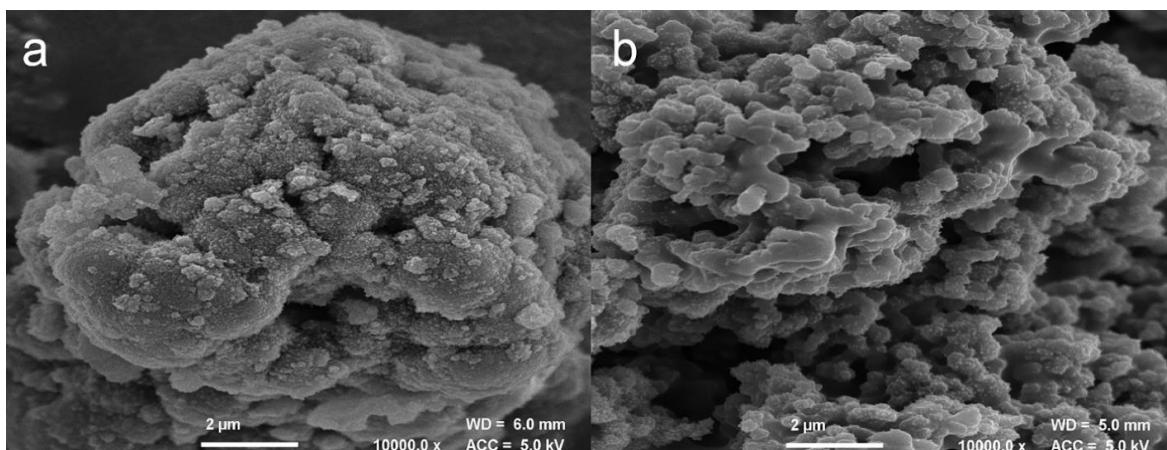
191

192 3. Results and Discussion

193 3.1. Characterization of PANI-EB and PANI-PAMPSA

194 FESEM images of PANI-EB and PANI-PAMPSA are shown in Figure 1. It can be
195 observed that the structure of PANI-EB is tightly packed, making it difficult to distinguish the size
196 and shape of individual particles (Figure 1(a)). This is in agreement with previous literature which
197 reported that PANI-EB tends to aggregate during the polymerization process [42]. In comparison,
198 the structure of PANI-PAMPSA is composed of porous particle aggregates (Figure 1(b)). The
199 FESEM image of PANI-PAMPSA at 150k magnification shows that the average diameter of the
200 particles is in the range of 50 and 100 nm (Figure S1). The porous structure of PANI-PAMPSA is
201 expected to provide a larger surface area and thus increase the dye adsorption in comparison to
202 PANI-EB.

203



204

205 Figure 1: FESEM images of (a) PANI-EB and (b) PANI-PAMPSA

206

207 Figure 2(a) shows the FTIR spectra of PANI-EB and PANI-PAMPSA. The typical bands
208 of PANI-EB are observed at 1586 cm^{-1} (quinoid C=C stretching), 1490 cm^{-1} (benzenoid C=C
209 stretching), 1378 cm^{-1} (quinoid C-N stretching), 1286 cm^{-1} (aromatic amine C-N stretching),
210 1156 cm^{-1} (aromatic imine C=N stretching) and 818 cm^{-1} (C-H bending) [43]. The bands of PANI-
211 PAMPSA at approximately 1641 cm^{-1} and 1032 cm^{-1} are attributed to the C=O stretching and the
212 symmetric O=S=O stretching, which correspond to the carbonyl and sulfonic groups of PAMPSA,
213 respectively [34]. It is noticeable that the bands of quinoid (1586 cm^{-1}) and benzenoid (1490 cm^{-1})
214 in PANI-EB show a red shift to 1546 cm^{-1} and 1440 cm^{-1} in the spectrum of PANI-PAMPSA.

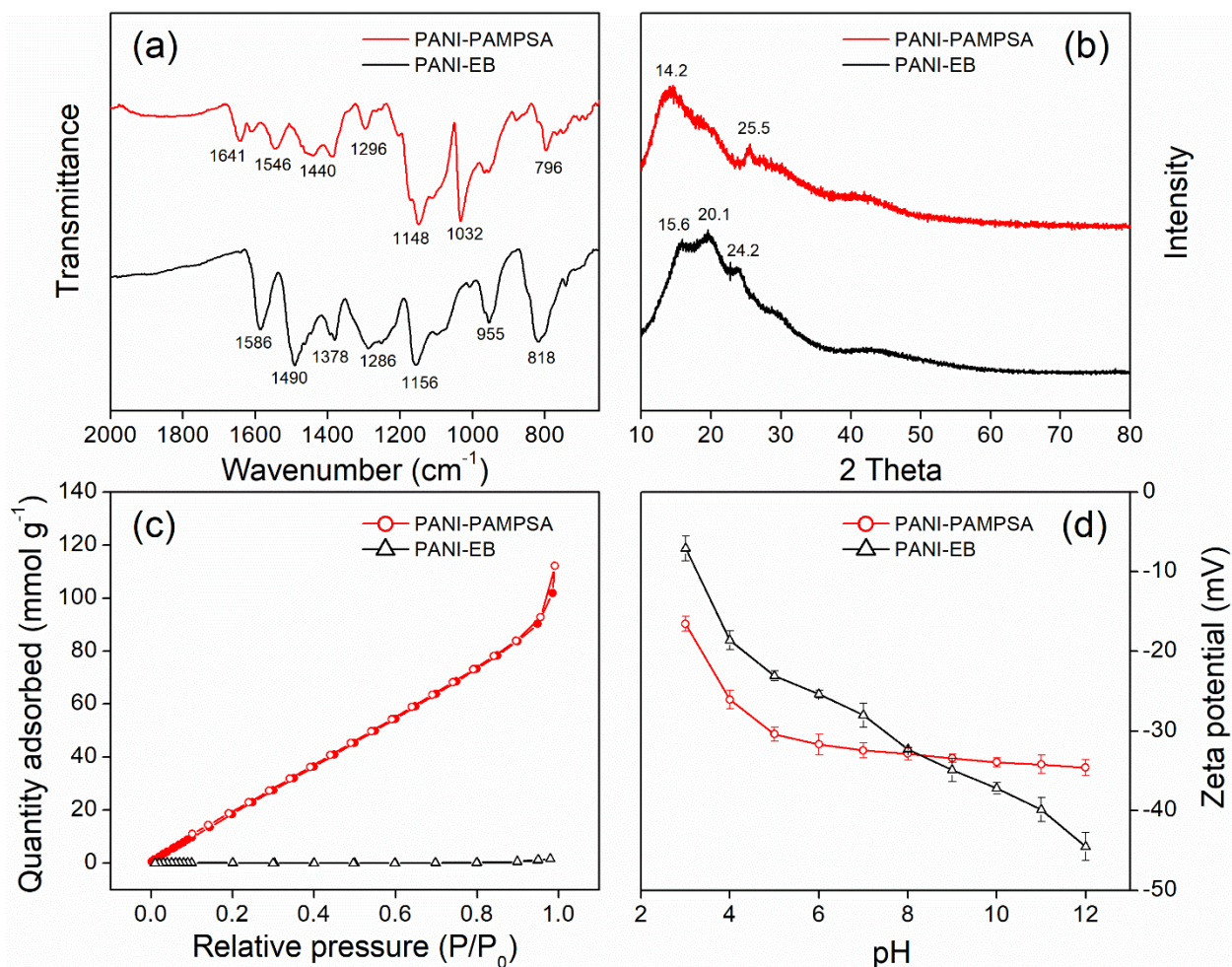
215 This indicates the interaction between the backbone of PANI and PAMPSA, which is associated
216 with the π -electron delocalization induced by protonation [18]. The bands at 1296 cm^{-1} and 1148
217 cm^{-1} are assigned to the protonated amine and protonated imine groups, respectively. The FTIR
218 results suggest that the incorporation of PAMPSA in PANI is through an interaction between
219 sulfonic groups of PAMPSA and nitrogen atoms of PANI [34].

220 Figure 2(b) shows the XRD patterns of PANI-EB and PANI-PAMPSA. The crystalline
221 phases of PANI-EB can be identified by some blunt peaks at 2θ values of 15.6° , 20.1° and 24.2° .
222 The peaks at 20.1° and 24.2° represent the reflection plane of (020) and (200) [44], corresponding
223 to the periodicity parallel and perpendicular to the polymer chain of PANI, respectively [45]. As
224 reported in literatures, most regions in the PANI structure are amorphous [46]. When PAMPSA
225 was doped into PANI, the XRD pattern shows two peaks at 14.2° and 25.5° , which may indicate
226 the rearrangement in the polymer chain of PANI due to the interaction with the PAMPSA
227 macromolecule [34]. The number and intensity of peaks in PANI-PAMPSA are both lower than
228 that in PANI-EB, representing a decrease in crystallinity. Given that PAMPSA is an amorphous
229 polymer, the incorporation of large amounts of PAMPSA would make ordering of PANI chains
230 difficult. The less-ordered structures of acid doped PANI in comparison to PANI-EB has
231 previously also been reported [42, 46].

232 Figure 2(c) displays the nitrogen physisorption (adsorption/desorption) isotherms for
233 PANI-EB and PANI-PAMPSA. The specific surface areas of the adsorbents can be calculated
234 from the physisorption isotherms using the BET theory. PANI-EB had a specific surface area of
235 $12\text{ m}^2\text{ g}^{-1}$, while PANI-PAMPSA had a higher specific surface area of $126\text{ m}^2\text{ g}^{-1}$. As reported in
236 the literature, PANI-EB with various morphologies obtained significantly different specific
237 surface areas, including conventional PANI-EB ($< 20\text{ m}^2\text{ g}^{-1}$) [47], nanostructured PANI-EB (24
238 $- 80\text{ m}^2\text{ g}^{-1}$) [48, 49], and crosslinked PANI-EB ($349 - 1083\text{ m}^2\text{ g}^{-1}$) [22, 23]. Nevertheless, the
239 specific surface area of PANI-PAMPSA has never been reported. This study shows that the
240 polyacid doping leads to a 10-fold increase in the specific surface area of PANI-EB, which concurs
241 with results of FESEM images in Figure 1. This is possibly because the PANI particles are located
242 along the PAMPSA macromolecule to form the double-strand structure during polymerization [34].
243 In the absence of PAMPSA, PANI-EB particles are susceptible to aggregation and hence, larger
244 particles with smaller specific surface areas are formed.

245 Figure 2(d) illustrates the variations of zeta potential of PANI-EB and PANI-PAMPSA in
246 the pH range 3 – 12. PANI-EB exhibits negative zeta potential at all pH values because it became
247 dedoped by the alkaline treatment. The zeta potential of PANI-PAMPSA also remains negative at
248 all pH values, and its absolute value increases from 16.5 mV (at pH = 3) to 34.6 mV (at pH = 12).
249 When in an acidic environment, PANI-PAMPSA is in the doped form where the backbone carries
250 positive charge [50]. However, the polymer matrix on the whole is negatively charged due to the
251 dissociation of the PAMPSA macromolecule ($pK_a = 0.87$). This is similar to the findings by
252 Mukherjee, Sharma, Saini and De [51] who found that PANI doped with an anionic surfactant,
253 dodecyl benzene sulfonic acid (DBSA), remained negatively charged from pH 2 to 12. With the
254 increase of the solution pH, the positive sites in PANI-PAMPSA get deprotonated, and the net
255 surface charge becomes more negative. It should be noted that PANI-PAMPSA shows a more
256 gradual increase in the absolute value of zeta potential compared to PANI-EB. This is because the
257 functional groups from PAMPSA, such as $-SO_3H$ and $-COOH$ groups, have buffer effects against
258 pH variations [52]. The zeta potential of PANI-PAMPSA is always below -30 mV between pH 5
259 and 12, which suggests a stable colloidal system that is resistant to particle aggregation and is
260 therefore beneficial to adsorption [53].

261



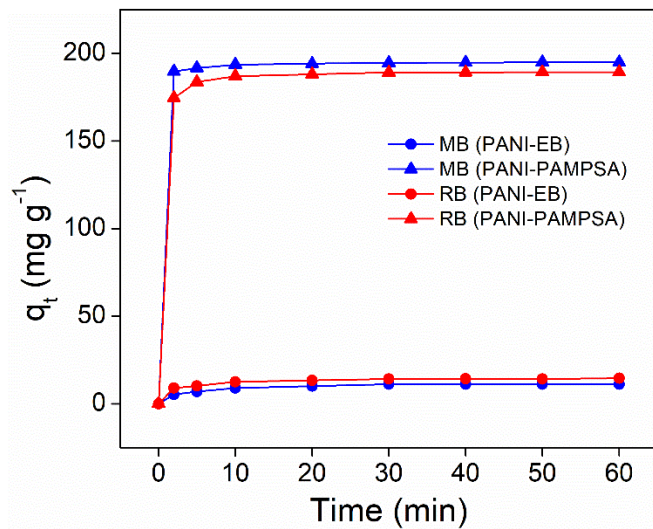
262
 263 Figure 2: (a) FTIR; (b) XRD; (c) N₂ sorption isotherms and (d) zeta potential of PANI-EB and
 264 PANI-PAMPSA
 265

266 3.2. Adsorption capacities of PANI-EB and PANI-PAMPSA

267 The adsorption capacity curves of PANI-EB and PANI-PAMPSA for MB and RB at
 268 different time intervals are shown in Figure 3. The adsorption process is extremely rapid in the
 269 initial 2 min, especially for PANI-PAMPSA. All the curves become flat after 10 min, indicating
 270 adsorption equilibrium is reached. PANI-EB shows relatively low adsorption capacities for MB
 271 (11.2 mg g⁻¹) and RB (14.5 mg g⁻¹), which are likely attributed to the particle aggregation and the
 272 small specific surface area. Compared to PANI-EB, PANI-PAMPSA possesses much higher
 273 adsorption capacities for both MB and RB. The adsorption capacity of PANI-PAMPSA for MB is
 274 194.9 mg g⁻¹, which is significantly higher than any other PANI-based materials, such as

275 nanostructured PANI-EB (4.8 mg g^{-1}) [20], crosslinked PANI-EB (6.9 mg g^{-1}) [22], and PANI-
276 nickel ferrite nanocomposite (6.6 mg g^{-1}) [54]. The adsorption capacity of PANI-PAMPSA for
277 RB is 189.4 mg g^{-1} . Although adsorption of RB by PANI-based materials has not been explored
278 previously, the result from this study is in general consistent with the above-mentioned adsorption
279 capacities of PANI-based materials for other anionic dyes [26, 32]. Another interesting finding is
280 that the equilibrium time of PANI-PAMPSA (approximately 10 min) is much faster than previous
281 studies that report equilibrium times in the range of 60 – 120 min [20, 23, 55], which is an
282 additional advantage for PANI-PAMPSA. These results demonstrate that PANI-PAMPSA can be
283 utilized as a very efficient adsorbent to remove both cationic and anionic dyes from aqueous
284 solutions.

285



286

287 Figure 3: Effect of contact time on adsorption capacity of PANI-EB and PANI-PAMPSA for MB
288 and RB (0.5 g L^{-1} adsorbent, 100 mg L^{-1} dye, $\text{pH} = 7$, $25 \text{ }^\circ\text{C}$)

289

290 3.3. *Effect of adsorbent dosage, initial dye concentration and solution pH*

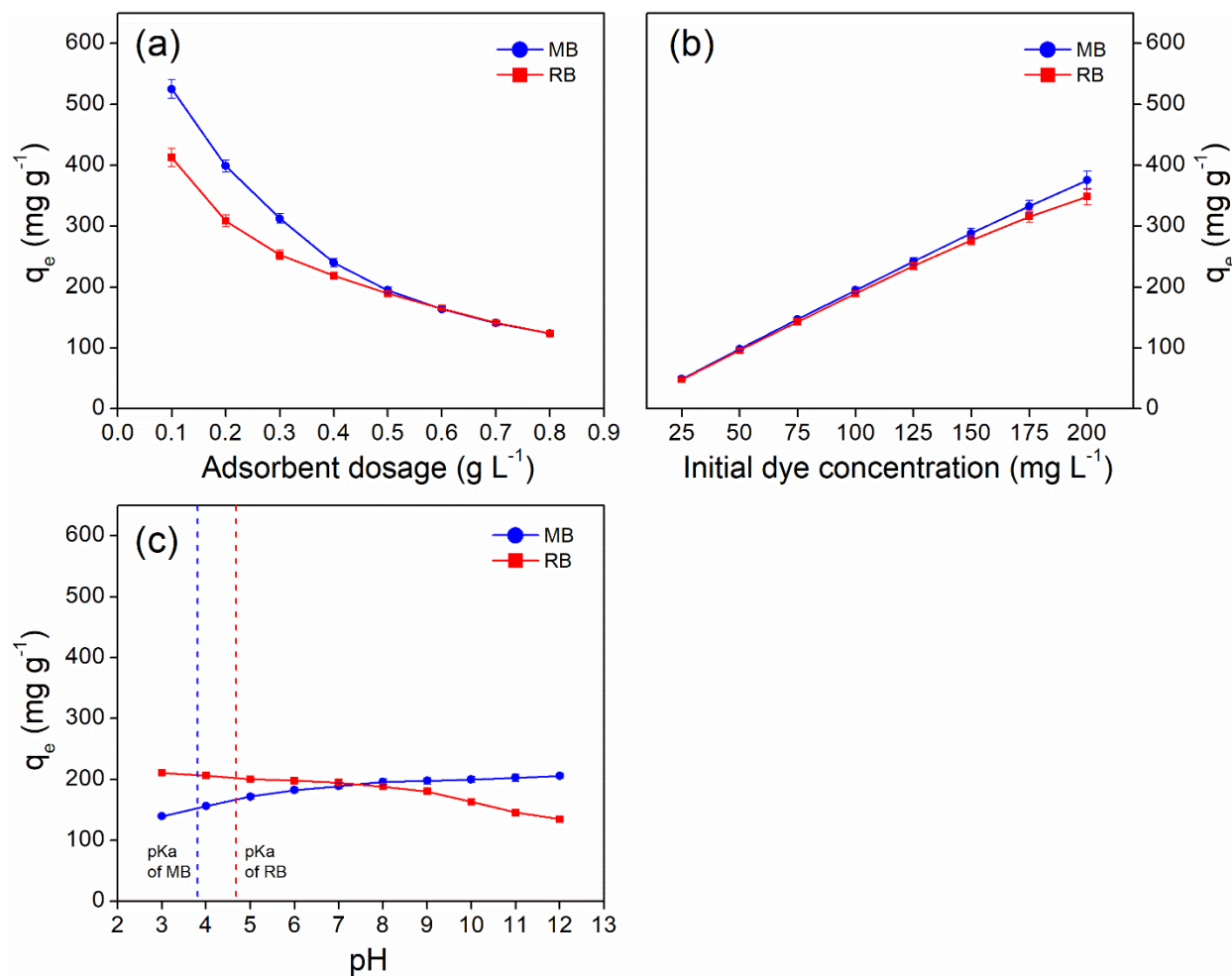
291 To observe the effect of adsorbent dosage on dye adsorption, 100 mg L^{-1} of MB or RB at
292 $\text{pH} = 7$, $25 \text{ }^\circ\text{C}$ was put in contact with various amounts of PANI-PAMPSA ($0.1 - 0.8 \text{ g L}^{-1}$). As
293 can be seen in Eq. (1), the adsorption capacity and the adsorbent dosage have an inverse
294 relationship. Figure 4(a) shows that when the amount of PANI-PAMPSA increases, the adsorption
295 capacities for both dyes decrease. This is because the adsorption sites available will not be fully
296 utilized at a higher adsorbent dosage in comparison to a lower adsorbent dosage [23, 56].

297 Maximum adsorption capacities for MB and RB are 525.2 and 412.7 mg g⁻¹ with PANI-PAMPSA
298 dosage of 0.1 g L⁻¹. When it comes to the percentage removal, 95% removal of both dyes can be
299 achieved with PANI-PAMPSA dosage of 0.5 g L⁻¹. Therefore, 0.5 g L⁻¹ was chosen as the fixed
300 dosage of PANI-PAMPSA for subsequent experiments.

301 The effect of initial dye concentration on the adsorption capacity of PANI-PAMPSA is
302 shown in Figure 4(b). The adsorption capacities for MB and RB increase almost linearly with the
303 initial dye concentration in the range of 25 to 200 mg L⁻¹. This can be explained by the increase
304 in the adsorbate to adsorbent ratio [23]. Previous studies found that the initial dye concentration is
305 the main driving force for mass transfer from solution to the adsorbent [2, 55, 57]. The higher the
306 initial dye concentration, the greater the driving force for adsorption, indicating stronger
307 interactions between dye molecules and available sites on the adsorbent surface [55]. The reduce
308 of linearity for RB at higher dye concentrations may suggest a nearly saturation limit for PANI-
309 PAMPSA [23]. A moderate initial dye concentration of 100 mg L⁻¹ was chosen as the fixed
310 adsorbate concentration for further study.

311 The solution pH plays a key role in the adsorption process, because it affects the surface
312 charge and active sites of the adsorbent, as well as the speciation of the adsorbate [56, 58]. At low
313 pH, both MB and RB are neutral. When the pH increases, MB becomes positively charged (pKa
314 = 3.8), and RB becomes negatively charged (pKa = 4.7) [59, 60]. Figure 2(d) shows that the
315 negative surface charge of PANI-PAMPSA increases from pH 3 to pH 12, which indicates the
316 stronger electrostatic interaction (attractive for MB and repulsive for RB) at higher side of pH.
317 Figure 4(c) plots the adsorption capacities of PANI-PAMPSA for MB and RB as a function of
318 solution pH. As expected from the zeta potential result, the adsorption capacity for MB gradually
319 increases from 139.3 to 205.8 mg g⁻¹, and that for RB decreases from 210.9 to 134.6 mg g⁻¹ with
320 an increase of pH from 3 to 12. Such opposite trends in ionic dyes has been previously reported
321 [23].

322



323
 324 Figure 4: Effect of (a) adsorbent dosage; (b) initial dye concentration; (c) solution pH on adsorption
 325 capacity of PANI-PAMPSA for MB and RB
 326

327 3.4. Adsorption kinetics, isotherms and thermodynamics

328 The adsorption kinetics is an important characteristic that provides information in regards
 329 to the controlling mechanisms of the adsorption process. The kinetics data were fitted into three
 330 kinetics models: pseudo-first-order (PFO) [61], pseudo-second-order (PSO) [62], and intraparticle
 331 diffusion (IPD) [63] models. The PFO and PSO models assume that the reaction at the liquid/solid
 332 interface is the limiting mechanism, while the IPD model assumes that the reaction is a very rapid
 333 process and the adsorption is controlled by intraparticle diffusion [64, 65]. The PFO, PSO and IPD
 334 models are expressed as Eq. (3), Eq. (4), and Eq. (5), respectively. q_t and q_e are the adsorption
 335 capacity (mg g^{-1}) of PANI-PAMPSA at time t and at equilibrium, k_1 is the PFO rate constant

336 (min^{-1}), k_2 is the PSO rate constant ($\text{g mg}^{-1} \text{min}^{-1}$), k_d is the IPD rate constant ($\text{mg g}^{-1} \text{min}^{-0.5}$),
337 and C is a constant indicating the thickness of the boundary layer. Non-linear forms of PFO and
338 PSO equations are used as they are found to be more suitable than the linear forms to determine
339 the kinetic parameters [66, 67].

340
341
$$q_t = q_e(1 - e^{-k_1 t}) \quad (3)$$

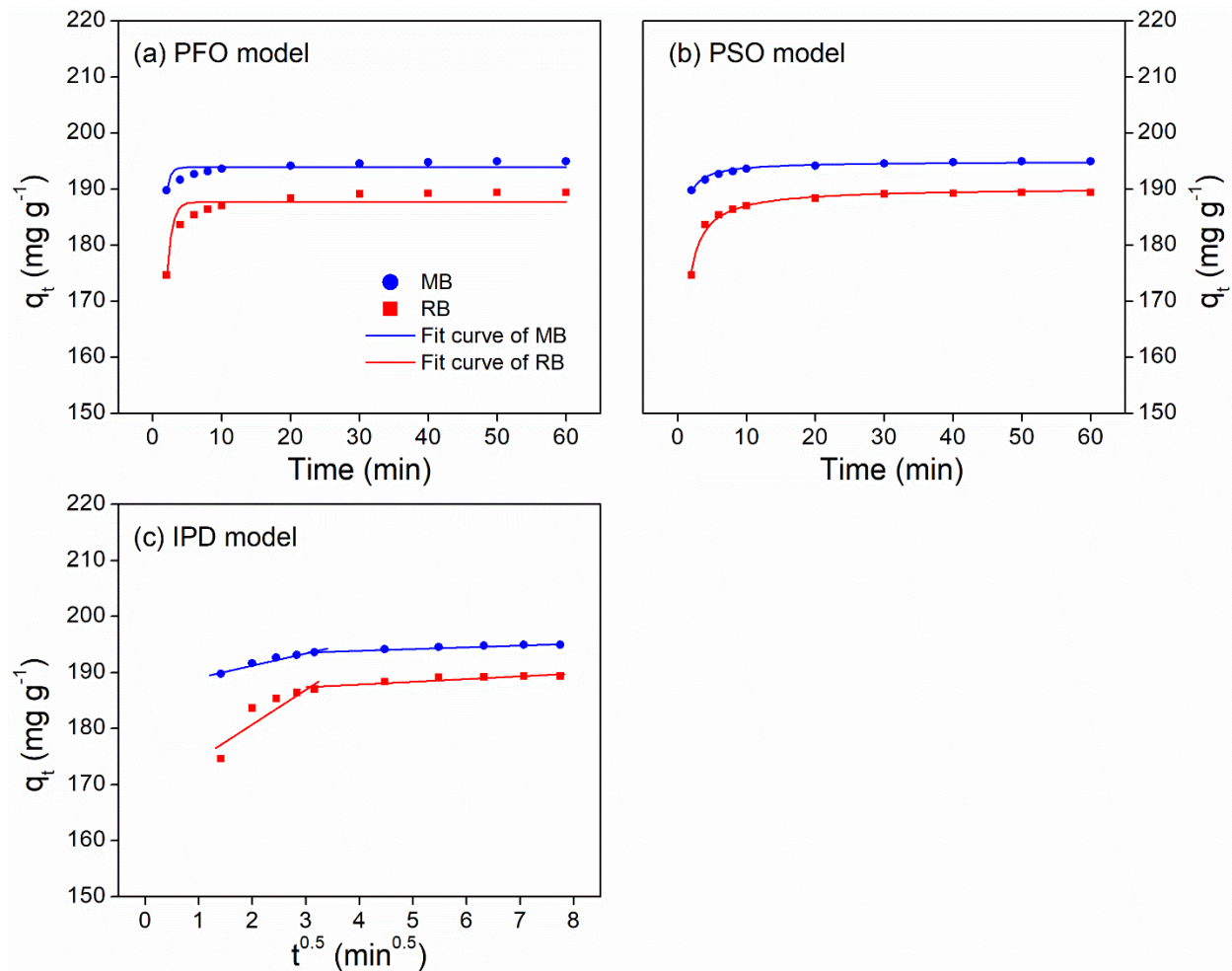
342
343
$$q_t = \frac{k_2 q_e^2 t}{1 + k_2 q_e t} \quad (4)$$

344
345
$$q_t = k_d t^{0.5} + C \quad (5)$$

346
347 The comparison of PSO and PFO models for adsorption of MB and RB respectively by
348 PANI-PAMPSA are shown in Figure 5(a) and Figure 5(b), and the corresponding kinetic
349 parameters and the correlation coefficient (R^2) are summarized in Table S2. The PSO model shows
350 a better fit for both MB and RB than the PFO model based on the R^2 values, and the calculated q_e
351 value agrees very well with the experimental value. Therefore, the adsorption kinetics of MB and
352 RB onto PANI-PAMPSA can be satisfactorily described by the PSO model. Such a finding is in
353 good agreement with previous studies [22-24, 32, 55, 68].

354 The possibility of intraparticle diffusion is explored by using the IPD model in Figure 5(c).
355 If the plot of q_t versus $t^{0.5}$ gives a straight line that passes through the origin of coordinates, then
356 the adsorption process is controlled by intraparticle diffusion only [69]. However, the data exhibit
357 multi-linear plots and the straight lines deviate from the origin. The first straight line depicts the
358 intraparticle diffusion of dye molecules in macropores of PANI-PAMPSA, and the second straight
359 line represents the diffusion in micropores [69, 70]. The result indicates that intraparticle diffusion
360 is not the controlling mechanism in the adsorption system.

361



362

363 Figure 5: Adsorption kinetics of RB and MB onto PANI-PAMPSA fitted by (a) PFO, (b) PSO,
 364 and (c) IPD models (0.5 g L⁻¹ adsorbent, 100 mg L⁻¹ dye, pH = 7, 25 °C)

365

366 The adsorption isotherms can be used to describe the equilibrium relationship between the
 367 adsorbent and the adsorbate at a constant temperature, and is thus important for optimization of
 368 the adsorption system. In this study, the adsorption isotherm data were fitted using the Langmuir
 369 [71] and the Freundlich [72] models. The Langmuir model describes monolayer adsorption at a
 370 homogeneous surface, while the Freundlich model describes multilayer adsorption on a
 371 heterogeneous system.

372 The non-linear form of the Langmuir model can be represented by Eq. (6) where q_m is the
 373 maximum adsorption capacity of the adsorbent (mg g⁻¹), and K_L is the Langmuir constant which
 374 is related to the energy of adsorption (L mg⁻¹).

375

376
$$q_e = \frac{K_L q_m C_e}{1 + K_L C_e} \quad (6)$$

377

378 The separation factor (R_L) of the Langmuir isotherm can be defined by Eq. (7). The value
379 of R_L indicates the adsorption nature which can be either irreversible ($R_L = 0$), favourable ($0 < R_L$
380 < 1), linear ($R_L = 1$), or unfavourable ($R_L > 1$) [73].

381

382
$$R_L = \frac{1}{1 + K_L c_0} \quad (7)$$

383

384 The non-linear form of the Freundlich model can be expressed as Eq. (8) where K_F is the
385 Freundlich constant ($\text{mg}^{1-(1/n)} \text{L}^{1/n} \text{g}^{-1}$), and n is the index number indicating the extent of
386 adsorption.

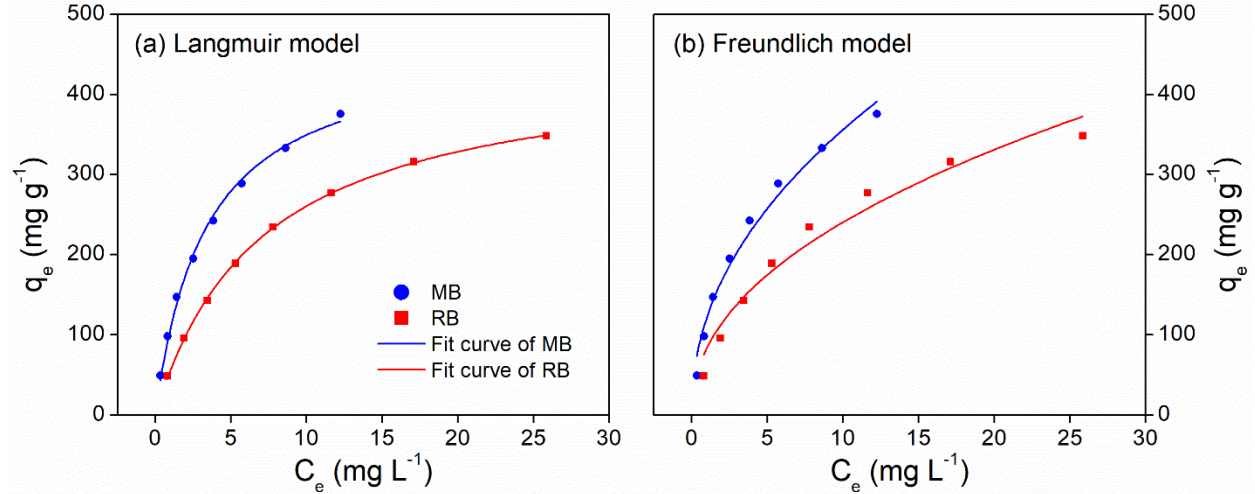
387

388
$$q_e = K_F C_e^{1/n} \quad (8)$$

389

390 The adsorption isotherms of MB and RB onto PANI-PAMPSA are shown in Figure 6 and
391 the parameters obtained are given in Table S3. It can be observed that the Langmuir model provide
392 a better fit to the experimental data in comparison to the Freundlich model. The values of R^2 of the
393 Langmuir model are closer to 1, showing that the Langmuir model explains the adsorption process
394 of both dyes better than the Freundlich model. This suggests that the adsorption of dyes on PANI-
395 PAMPSA follows a monolayer coverage adsorption mechanism [23, 74]. Figure S2 shows the
396 variation of R_L with the initial dye concentration. The R_L value lies between 0.01 and 0.12 for MB,
397 and between 0.03 and 0.22 for RB. This indicates the favourable adsorption of both dyes onto
398 PANI-PAMPSA. The maximum adsorption capacities of PANI-PAMPSA based on the Langmuir
399 model are 466.5 mg g^{-1} for MB, and 440.0 mg g^{-1} for RB, when the adsorbent dose is 0.5 g L^{-1}
400 and the temperature is $25 \text{ }^\circ\text{C}$. To our knowledge, PANI-PAMPSA has higher adsorption capacities
401 than any other PANI-based materials (Table 1), and is among the most effective adsorbents for
402 dye removal (such as commercial activated carbon and chitosan) [1, 2].

403



404

405 Figure 6: Adsorption isotherms of RB and MB onto PANI-PAMPSA fitted by (a) Langmuir and
 406 (b) Freundlich models (0.5 g L⁻¹ adsorbent, pH = 7, 25 °C)

407

408

409

410

411

412

413

414

415

416

417

418

419

420

421

422

423

424

425

To investigate whether the adsorption process is spontaneous or not, four sets of adsorption experiments were conducted at various temperatures from 298 to 318 K. The thermodynamic parameters are calculated as per Eq. (9) and Eq. (10), where ΔG° is the standard free energy change (kJ mol⁻¹), T is the temperature (K), R is the universal gas constant (8.314 J mol⁻¹ K⁻¹), K_0 is the adsorption equilibrium constant, ΔH° is the standard enthalpy change (kJ mol⁻¹), and ΔS° is the standard entropy change (kJ mol⁻¹ K⁻¹). K_0 was determined by plotting $\ln(q_e/c_e)$ versus c_e at different temperatures and extrapolating c_e to zero [75]. The values of ΔH° and ΔS° were calculated from the slope and intercept of the plot of $\ln K_0$ versus $1/T$, respectively.

$$\Delta G^\circ = -RT \ln K_0 \quad (9)$$

$$\ln K_0 = \frac{\Delta S^\circ}{R} - \frac{\Delta H^\circ}{RT} \quad (10)$$

The values of the thermodynamic parameters are given in Table 2. The negative values of ΔG° measured at all temperatures indicate that the adsorption process is thermodynamically spontaneous [76]. With an increase in temperature, the absolute value of ΔG° increases gradually, implying that the adsorption process is more favourable at higher temperature. The positive values of ΔH° confirm the endothermic nature of the adsorption process [77]. The positive values of ΔS°

426 imply an increase in the randomness at the adsorbent and adsorbate interface [78], which reflects
 427 a good affinity of the PANI-PAMPSA surface towards dye molecules. Additionally, the type of
 428 adsorption (physisorption and chemisorption) can be classified to a certain extent by the
 429 thermodynamic parameters. Generally, ΔG° for physisorption is between -20 and 0 kJ mol^{-1} , and
 430 for chemisorption is between -80 and -400 kJ mol^{-1} [79]. ΔH° due to physisorption is less than
 431 84 kJ mol^{-1} , while ΔH° due to chemisorption takes value between 84 and 420 kJ mol^{-1} [80].
 432 Therefore, the values of ΔG° and ΔH° in Table 2 both suggest that adsorption of dyes onto PANI-
 433 PAMPSA was driven by a physisorption process.

434

435 Table 2: Thermodynamic parameters of dye adsorption onto PANI-PAMPSA (0.5 g L^{-1} adsorbent,
 436 $\text{pH} = 7$)

Dye	$\Delta G^\circ (\text{kJ mol}^{-1})$				$\Delta H^\circ (\text{kJ mol}^{-1})$	$\Delta S^\circ (\text{kJ mol}^{-1} \text{ K}^{-1})$
	298 K	308 K	318 K	328 K		
MB	-11.89	-12.52	-13.28	-14.12	10.31	0.07
RB	-9.82	-10.49	-11.16	-11.73	9.20	0.06

437

438 3.5. Adsorption mechanisms

439 The adsorption of organic dyes on PANI-based materials in general follows mechanisms
 440 such as π - π interaction, electrostatic interaction, and hydrogen bonding [19, 23, 24]. As mentioned
 441 above, the adsorption of MB and RB follows the monolayer coverage mechanism, which rules out
 442 the possibility of hydrogen bonding because intermolecular hydrogen bonding between dye
 443 molecules would cause multilayer adsorption [74, 81]. At $\text{pH} = 3$ when the dyes are neutral and
 444 the electrostatic interaction between dye and PANI-PAMPSA is shielded, the adsorption capacities
 445 are still pretty high (139.3 mg g^{-1} for MB and 210.9 mg g^{-1} for RB). This suggests that the most
 446 possible driving force for the adsorption of dyes is the π - π interaction between aromatic rings of
 447 PANI-PAMPSA and dye molecules [74, 82]. On the other hand, as shown in Figure 4(c), at $\text{pH} =$
 448 12 when the electrostatic interaction (attractive for MB and repulsive for RB) and π - π interaction
 449 coexist, the adsorption capacity for MB is increased by 48%, and that for RB is decreased by 36%,
 450 in comparison to those at $\text{pH} = 3$. This indicates that electrostatic interaction also plays an
 451 important role in the adsorption of ionic dyes.

452 In order to prove the adsorption mechanisms, the FTIR spectra of PANI-PAMSPA before
453 and after dye adsorption were compared (Figure 7). The nitrogen atom of PANI interacts with the
454 sulfonic groups of PAMPSA and this causes more delocalization (two vibrational bands of C-N
455 stretching of secondary aromatic amine [34]). In the MB-loaded PANI-PAMPSA, these peaks
456 overlap with the intense vibrational bands of C-N stretching and CH₃ stretching of the dye, making
457 it difficult to determine the nature of the interaction. The bands due to S=O stretching shift from
458 1153 – 1034 to 1109 – 1025 and this is possibly due to electron delocalization caused by
459 electrostatic interaction between MB and the PANI-PAMPSA [23]. In the RB-loaded PANI-
460 PAMPSA, the vibrational band due to the quinoid C=C stretching of PANI-PAMPSA shifts from
461 1546 to 1563 cm⁻¹, which is due to π - π interaction between the localized π electrons in the aromatic
462 rings of PANI-PAMPSA and RB. Therefore, the main adsorption mechanism of PANI-PAMPSA
463 towards both anionic and cationic dyes is π - π interaction while electrostatic interaction has an
464 additional attractive and repulsive effect on cationic and anionic dyes, respectively.

465

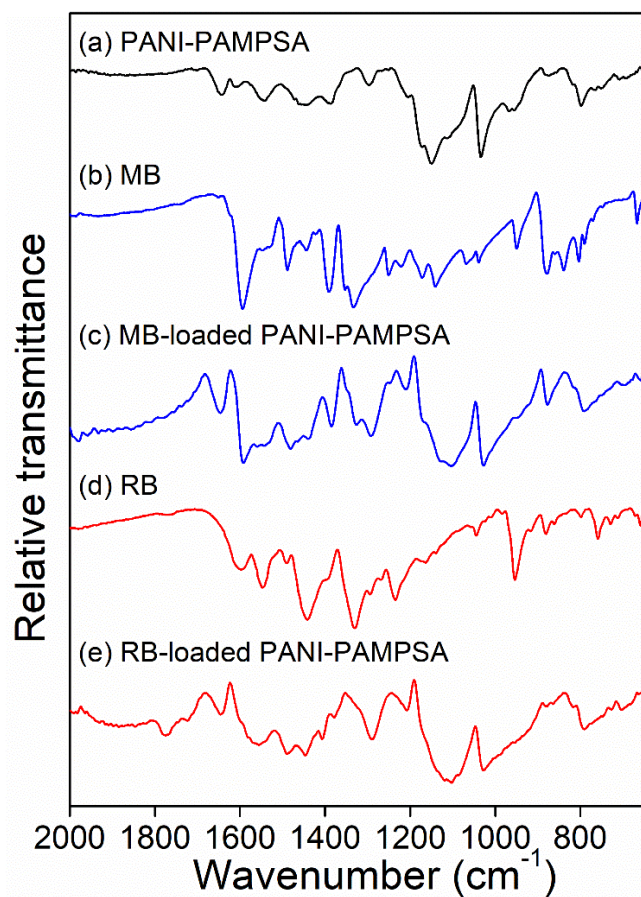
466

467

468

469

470



471
 472 Figure 7: FTIR of spectra of (a) PANI-PAMPSA, (b) MB, (c) MB-loaded PANI-PAMPSA, (d)
 473 RB, and (e) RB-loaded PANI-PAMPSA

474

475 **4. Conclusions**

476 In this study, a polyacid doped PANI adsorbent PANI-PAMPSA was used for dye removal
 477 for the first time. PANI-PAMPSA was synthesized by matrix polymerization of aniline in the
 478 presence of the polyacid PAMPSA. FTIR and XRD results evidenced the successful incorporation
 479 of PAMPSA in PANI. FESEM and BET analysis showed that PAMPSA was of great importance
 480 for the formation of the porous structure of PANI-PAMPSA, which had a specific surface area of
 481 $126 \text{ m}^2 \text{ g}^{-1}$. Adsorption experiments showed that PANI-PAMPSA could substantially remove both
 482 cationic (MB) and anionic (RB) dyes from the aqueous solution, while PANI-EB was not effective
 483 for dye adsorption. The adsorption capacities of PANI-PAMPSA were significantly influenced by
 484 the adsorbent dosage, the initial dye concentration, and the solution pH. The adsorption kinetics
 485 obeyed the PSO model, and the isotherms followed the Langmuir monolayer model. Based on the

486 Langmuir isotherm, the maximum adsorption capacities of PANI-PAMPSA were 466.5 mg g⁻¹
487 and 440.0 mg g⁻¹ for MB and RB, respectively. These values were significantly higher than other
488 previously reported PANI-based materials. The thermodynamic parameters suggested that the
489 adsorption process was spontaneous and endothermic in nature. The adsorption mechanisms
490 included π - π interaction and electrostatic interaction between the dyes and the adsorbent. This
491 work not only presented a promising PANI adsorbent for organic dyes, but also shed some light
492 on the development of other conducting polymer-based adsorbents for wastewater treatment. For
493 large-scale applications, this adsorbent can be used in a combined adsorption-filtration process, or
494 be used as adsorptive membranes.

495

496 **5. Acknowledgements**

497 This work was supported by the European Research Council (ERC) Consolidator grant
498 TUNEMEM (Project reference: 646769; funded under H2020-EU.1.1.-EXCELLENT SCIENCE).
499 The authors thank Dr. Gabriele Kociok-Köhn and Dr Philip Fletcher (University of Bath) for XRD
500 and FESEM analysis, and the technician team at the Department of Chemical Engineering,
501 University of Bath for technical support.

502

503 **References**

- 504 [1] V.K. Gupta, Suhas, Application of low-cost adsorbents for dye removal – A review, *J. Environ.*
505 *Manage.*, 90 (2009) 2313-2342.
- 506 [2] M.T. Yagub, T.K. Sen, S. Afroze, H.M. Ang, Dye and its removal from aqueous solution by
507 adsorption: A review, *Adv. Colloid Interface Sci.*, 209 (2014) 172-184.
- 508 [3] A. Pirkarami, M.E. Olya, Removal of dye from industrial wastewater with an emphasis on
509 improving economic efficiency and degradation mechanism, *J. Saudi Chem. Soc.*, 21 (2017) S179-
510 S186.
- 511 [4] G.E. Walsh, L.H. Bahner, W.B. Horning, Toxicity of textile mill effluents to freshwater and
512 estuarine algae, crustaceans and fishes, *Environ. Pollut. A*, 21 (1980) 169-179.
- 513 [5] W.G. Kuo, Decolorizing dye wastewater with Fenton's reagent, *Water Res.*, 26 (1992) 881-
514 886.

- 515 [6] S. Sadri Moghaddam, M.R. Alavi Moghaddam, M. Arami, Coagulation/flocculation process
516 for dye removal using sludge from water treatment plant: Optimization through response surface
517 methodology, *J. Hazard. Mater.*, 175 (2010) 651-657.
- 518 [7] S. Yu, M. Liu, M. Ma, M. Qi, Z. Lü, C. Gao, Impacts of membrane properties on reactive dye
519 removal from dye/salt mixtures by asymmetric cellulose acetate and composite polyamide
520 nanofiltration membranes, *J. Membr. Sci.*, 350 (2010) 83-91.
- 521 [8] S. Wang, A comparative study of Fenton and Fenton-like reaction kinetics in decolourisation
522 of wastewater, *Dyes Pigm.*, 76 (2008) 714-720.
- 523 [9] Ö. Gerçel, Removal of textile dye from aqueous solution by electrochemical method, *Sep. Sci.*
524 *Technol.*, 51 (2016) 711-717.
- 525 [10] V.K. Gupta, R. Jain, A. Mittal, M. Mathur, S. Sikarwar, Photochemical degradation of the
526 hazardous dye Safranin-T using TiO₂ catalyst, *J. Colloid Interface Sci.*, 309 (2007) 464-469.
- 527 [11] A. Kausar, M. Iqbal, A. Javed, K. Aftab, Z.-i.-H. Nazli, H.N. Bhatti, S. Nouren, Dyes
528 adsorption using clay and modified clay: A review, *J. Mol. Liq.*, 256 (2018) 395-407.
- 529 [12] Y. Huang, J. Li, X. Chen, X. Wang, Applications of conjugated polymer based composites in
530 wastewater purification, *RSC Adv.*, 4 (2014) 62160-62178.
- 531 [13] M. Wan, J. Yang, Mechanism of proton doping in polyaniline, *J. Appl. Polym. Sci.*, 55 (1995)
532 399-405.
- 533 [14] D.W. Hatchett, M. Josowicz, J. Janata, Acid doping of polyaniline: Spectroscopic and
534 electrochemical studies, *J. Phys. Chem. B*, 103 (1999) 10992-10998.
- 535 [15] A.N. Chowdhury, S.R. Jesmeen, M.M. Hossain, Removal of dyes from water by conducting
536 polymeric adsorbent, *Polym. Adv. Technol.*, 15 (2004) 633-638.
- 537 [16] E.N. Zare, A. Motahari, M. Sillanpää, Nanoadsorbents based on conducting polymer
538 nanocomposites with main focus on polyaniline and its derivatives for removal of heavy metal
539 ions/dyes: A review, *Environ. Res.*, 162 (2018) 173-195.
- 540 [17] Y. Moo Lee, S. Yong Nam, S. Yong Ha, Pervaporation of water/isopropanol mixtures through
541 polyaniline membranes doped with poly(acrylic acid), *J. Membr. Sci.*, 159 (1999) 41-46.
- 542 [18] L. Xu, Electrically Tuneable Membranes: Revolutionising Separation and Fouling Control
543 for Membrane Reactors, Department of Chemical Engineering, University of Bath, UK, 2016.
- 544 [19] M. Ayad, G. El-Hefnawy, S. Zaghlol, Facile synthesis of polyaniline nanoparticles; its
545 adsorption behavior, *Chem. Eng. J.*, 217 (2013) 460-465.
- 546 [20] M.M. Ayad, A.A. El-Nasr, Adsorption of cationic dye (Methylene Blue) from water using
547 polyaniline nanotubes base, *J. Phys. Chem. C*, 114 (2010) 14377-14383.

- 548 [21] M.M. Ayad, A. Abu El-Nasr, J. Stejskal, Kinetics and isotherm studies of methylene blue
549 adsorption onto polyaniline nanotubes base/silica composite, *J. Ind. Eng. Chem.*, 18 (2012) 1964-
550 1969.
- 551 [22] M. Ayad, S. Zaghlol, Nanostructured crosslinked polyaniline with high surface area:
552 Synthesis, characterization and adsorption for organic dye, *Chem. Eng. J.*, 204-206 (2012) 79-86.
- 553 [23] V. Sharma, P. Rekha, P. Mohanty, Nanoporous hypercrosslinked polyaniline: An efficient
554 adsorbent for the adsorptive removal of cationic and anionic dyes, *J. Mol. Liq.*, 222 (2016) 1091-
555 1100.
- 556 [24] L. Ai, J. Jiang, R. Zhang, Uniform polyaniline microspheres: A novel adsorbent for dye
557 removal from aqueous solution, *Synth. Met.*, 160 (2010) 762-767.
- 558 [25] S. Agarwal, I. Tyagi, V.K. Gupta, F. Golbaz, A.N. Golikand, O. Moradi, Synthesis and
559 characteristics of polyaniline/zirconium oxide conductive nanocomposite for dye adsorption
560 application, *J. Mol. Liq.*, 218 (2016) 494-498.
- 561 [26] D. Mahanta, G. Madras, S. Radhakrishnan, S. Patil, Adsorption of sulfonated dyes by
562 polyaniline emeraldine salt and its kinetics, *J. Phys. Chem. B*, 112 (2008) 10153-10157.
- 563 [27] V. Janaki, B.-T. Oh, K. Shanthi, K.-J. Lee, A.K. Ramasamy, S. Kamala-Kannan,
564 Polyaniline/chitosan composite: An eco-friendly polymer for enhanced removal of dyes from
565 aqueous solution, *Synth. Met.*, 162 (2012) 974-980.
- 566 [28] P. Gharbani, Synthesis of polyaniline-tin(II)molybdophosphate nanocomposite and
567 application of it in the removal of dyes from aqueous solutions, *J. Mol. Liq.*, 242 (2017) 229-234.
- 568 [29] V.K. Gupta, D. Pathania, N.C. Kothiyal, G. Sharma, Polyaniline zirconium (IV)
569 silicophosphate nanocomposite for remediation of methylene blue dye from waste water, *J. Mol.*
570 *Liq.*, 190 (2014) 139-145.
- 571 [30] M. Tanzifi, S.H. Hosseini, A.D. Kiadehi, M. Olazar, K. Karimipour, R. Rezaiemehr, I. Ali,
572 Artificial neural network optimization for methyl orange adsorption onto polyaniline nano-
573 adsorbent: Kinetic, isotherm and thermodynamic studies, *J. Mol. Liq.*, 244 (2017) 189-200.
- 574 [31] B. Yan, Z. Chen, L. Cai, Z. Chen, J. Fu, Q. Xu, Fabrication of polyaniline hydrogel: Synthesis,
575 characterization and adsorption of methylene blue, *Appl. Surf. Sci.*, 356 (2015) 39-47.
- 576 [32] D. Mahanta, G. Madras, S. Radhakrishnan, S. Patil, Adsorption and desorption kinetics of
577 anionic dyes on doped polyaniline, *J. Phys. Chem. B*, 113 (2009) 2293-2299.
- 578 [33] Y. Xia, T. Li, J. Chen, C. Cai, Polyaniline (skin)/polyamide 6 (core) composite fiber:
579 Preparation, characterization and application as a dye adsorbent, *Synth. Met.*, 175 (2013) 163-169.
- 580 [34] O.L. Gribkova, A.A. Nekrasov, M. Trchova, V.F. Ivanov, V.I. Sazikov, A.B. Razova, V.A.
581 Tverskoy, A.V. Vannikov, Chemical synthesis of polyaniline in the presence of

582 poly(amidosulfonic acids) with different rigidity of the polymer chain, *Polymer*, 52 (2011) 2474-
583 2484.

584 [35] M.A. Guseva, A.A. Isakova, O.L. Gribkova, V.A. Tverskoi, V.F. Ivanov, A.V. Vannikov,
585 Y.A. Fedotov, Matrix polymerization of aniline in the presence of polyamides containing sulfo
586 acid groups, *Polym. Sci. A*, 49 (2007) 4-11.

587 [36] J.-W. Jeon, Y. Ma, J.F. Mike, L. Shao, P.B. Balbuena, J.L. Lutkenhaus, Oxidatively stable
588 polyaniline:polyacid electrodes for electrochemical energy storage, *PCCP*, 15 (2013) 9654-9662.

589 [37] J. Shen, S. Shahid, A. Sarihan, D.A. Patterson, E.A.C. Emanuelsson, Effect of polyacid
590 dopants on the performance of polyaniline membranes in organic solvent nanofiltration, *Sep. Purif.*
591 *Technol.*, 204 (2018) 336-344.

592 [38] V.F. Ivanov, O.L. Gribkova, K.V. Cheberyako, A.A. Nekrasov, V.A. Tverskoi, A.V.
593 Vannikov, Template synthesis of polyaniline in the presence of poly-(2-acrylamido-2-methyl-1-
594 propanesulfonic acid), *Russ. J. Electrochem.*, 40 (2004) 299-304.

595 [39] S. Bhadra, D. Khastgir, N.K. Singha, J.H. Lee, Progress in preparation, processing and
596 applications of polyaniline, *Prog. Polym. Sci.*, 34 (2009) 783-810.

597 [40] Z.A. Boeva, V.G. Sergeyev, Polyaniline: Synthesis, properties, and application, *Polym. Sci.*
598 *C*, 56 (2014) 144-153.

599 [41] British Standards Institution, Determination of the specific surface area of powders-part 1:
600 BET method of gas adsorption for solids (including porous materials), 1996.

601 [42] M.A.C. Mazzeu, L.K. Faria, A.d.M. Cardoso, A.M. Gama, M.R. Baldan, E.S. Gonçalves,
602 Structural and morphological characteristics of polyaniline synthesized in pilot scale, *J. Aerosp.*
603 *Technol. Manag.*, 9 (2017) 39-47.

604 [43] J. Jang, J. Ha, J. Cho, Fabrication of water-dispersible polyaniline-poly(4-styrenesulfonate)
605 nanoparticles for inkjet-printed chemical-sensor applications, *Adv. Mater.*, 19 (2007) 1772-1775.

606 [44] Z.-J. Gu, Q. Shen, Synthesis, characterization and comparison of polyaniline 1D-structure
607 controlled by poly(l-lactide) and poly(d-lactide), *Superlattices Microstruct.*, 89 (2016) 53-58.

608 [45] L. Shi, X. Wang, L. Lu, X. Yang, X. Wu, Preparation of TiO₂/polyaniline nanocomposite
609 from a lyotropic liquid crystalline solution, *Synth. Met.*, 159 (2009) 2525-2529.

610 [46] Zeghioud Hichem, Lamouri Saad, Safidine Zitouni, B. Mohammed, Chemical synthesis and
611 characterization of highly soluble conducting polyaniline in the mixtures of common solvents, *J.*
612 *Serb. Chem. Soc.*, 80 (2015) 917-931.

613 [47] K. Zarrini, A.A. Rahimi, F. Alihosseini, H. Fashandi, Highly efficient dye adsorbent based
614 on polyaniline-coated nylon-6 nanofibers, *J. Clean. Prod.*, 142 (2017) 3645-3654.

- 615 [48] M. Trchová, E.N. Konyushenko, J. Stejskal, J. Kovářová, G. Ćirić-Marjanović, The
616 conversion of polyaniline nanotubes to nitrogen-containing carbon nanotubes and their
617 comparison with multi-walled carbon nanotubes, *Polym. Degrad. Stab.*, 94 (2009) 929-938.
- 618 [49] J. Du, Z. Liu, B. Han, Z. Li, J. Zhang, Y. Huang, One-pot synthesis of the macroporous
619 polyaniline microspheres and Ag/polyaniline core-shell particles, *Microporous Mesoporous*
620 *Mater.*, 84 (2005) 254-260.
- 621 [50] Y. Wang, X.N. Guan, C.-Y. Wu, M.-T. Chen, H.-H. Hsieh, H.D. Tran, S.-C. Huang, R.B.
622 Kaner, Processable colloidal dispersions of polyaniline-based copolymers for transparent
623 electrodes, *Polymer Chemistry*, 4 (2013) 4814-4820.
- 624 [51] R. Mukherjee, R. Sharma, P. Saini, S. De, Nanostructured polyaniline incorporated
625 ultrafiltration membrane for desalination of brackish water, *Environ. Sci.: Water Res. Technol.*, 1
626 (2015) 893-904.
- 627 [52] H. Cui, Y. Qian, H. An, C. Sun, J. Zhai, Q. Li, Electrochemical removal of fluoride from
628 water by PAOA-modified carbon felt electrodes in a continuous flow reactor, *Water Res.*, 46 (2012)
629 3943-3950.
- 630 [53] O. Duman, S. Tunç, Electrokinetic and rheological properties of Na-bentonite in some
631 electrolyte solutions, *Microporous Mesoporous Mater.*, 117 (2009) 331-338.
- 632 [54] M.R. Patil, V.S. Shrivastava, Adsorptive removal of methylene blue from aqueous solution
633 by polyaniline-nickel ferrite nanocomposite: a kinetic approach, *Desalination Water Treat.*, 57
634 (2016) 5879-5887.
- 635 [55] B.N. Patra, D. Majhi, Removal of anionic dyes from water by potash alum doped polyaniline:
636 Investigation of kinetics and thermodynamic parameters of adsorption, *J. Phys. Chem. B*, 119
637 (2015) 8154-8164.
- 638 [56] J. Shen, M.F. Evangelista, G. Mkongo, H. Wen, R. Langford, G. Rosair, M.R.S. McCoustra,
639 V. Arrighi, Efficient defluoridation of water by Monetite nanorods, *Adsorption*, 24 (2018) 135-
640 145.
- 641 [57] Y. Bulut, H. Aydın, A kinetics and thermodynamics study of methylene blue adsorption on
642 wheat shells, *Desalination*, 194 (2006) 259-267.
- 643 [58] C. Sairam Sundaram, N. Viswanathan, S. Meenakshi, Defluoridation chemistry of synthetic
644 hydroxyapatite at nano scale: Equilibrium and kinetic studies, *J. Hazard. Mater.*, 155 (2008) 206-
645 215.
- 646 [59] X. He, K.B. Male, P.N. Nesterenko, D. Brabazon, B. Paull, J.H.T. Luong, Adsorption and
647 desorption of Methylene Blue on porous carbon monoliths and nanocrystalline cellulose, *ACS*
648 *Appl. Mater. Interfaces*, 5 (2013) 8796-8804.
- 649 [60] R.W. Sabnis, *Handbook of Biological Dyes and Stains: Synthesis and Industrial Applications*,
650 John Wiley & Sons, Inc., USA, 2010.

- 651 [61] S. Lagergren, About the theory of so-called adsorption of soluble substances, *Kungliga*
652 *Svenska Vetenskapsakademiens Handlingar*, 24 (1898) 1-39.
- 653 [62] Y.S. Ho, G. McKay, Pseudo-second order model for sorption processes, *Process Biochem.*,
654 34 (1999) 451-465.
- 655 [63] W.J. Weber, J.C. Morris, Kinetics of adsorption on carbon from solutions, *J. Sanit. Eng. Div.*,
656 89 (1963) 31-60.
- 657 [64] J.-P. Simonin, On the comparison of pseudo-first order and pseudo-second order rate laws in
658 the modeling of adsorption kinetics, *Chem. Eng. J.*, 300 (2016) 254-263.
- 659 [65] F.-C. Wu, R.-L. Tseng, R.-S. Juang, Initial behavior of intraparticle diffusion model used in
660 the description of adsorption kinetics, *Chem. Eng. J.*, 153 (2009) 1-8.
- 661 [66] K.V. Kumar, Linear and non-linear regression analysis for the sorption kinetics of methylene
662 blue onto activated carbon, *J. Hazard. Mater.*, 137 (2006) 1538-1544.
- 663 [67] J. Lin, L. Wang, Comparison between linear and non-linear forms of pseudo-first-order and
664 pseudo-second-order adsorption kinetic models for the removal of methylene blue by activated
665 carbon, *Front. Environ. Sci. Eng. Chin*, 3 (2009) 320-324.
- 666 [68] M.H. Mohamed, A. Dolatkah, T. Aboumourad, L. Dehabadi, L.D. Wilson, Investigation of
667 templated and supported polyaniline adsorbent materials, *RSC Adv.*, 5 (2015) 6976-6984.
- 668 [69] V. Fierro, V. Torné-Fernández, D. Montané, A. Celzard, Adsorption of phenol onto activated
669 carbons having different textural and surface properties, *Microporous Mesoporous Mater.*, 111
670 (2008) 276-284.
- 671 [70] A. Witek-Krowiak, Analysis of influence of process conditions on kinetics of malachite green
672 biosorption onto beech sawdust, *Chem. Eng. J.*, 171 (2011) 976-985.
- 673 [71] I. Langmuir, The adsorption of gases on plane surfaces of glass, mica and platinum, *J. Am.*
674 *Chem. Soc.*, 40 (1918) 1361-1403.
- 675 [72] C.-h. Yang, Statistical mechanical study on the Freundlich isotherm equation, *J. Colloid*
676 *Interface Sci.*, 208 (1998) 379-387.
- 677 [73] T.W. Weber, R.K. Chakravorti, Pore and solid diffusion models for fixed-bed adsorbers,
678 *AIChE J.*, 20 (1974) 228-238.
- 679 [74] J. Xiao, W. Lv, Z. Xie, Y. Tan, Y. Song, Q. Zheng, Environmentally friendly reduced
680 graphene oxide as a broad-spectrum adsorbent for anionic and cationic dyes via π - π interactions,
681 *J. Mater. Chem. A*, 4 (2016) 12126-12135.
- 682 [75] A.A. Khan, R.P. Singh, Adsorption thermodynamics of carbofuran on Sn (IV) arsenosilicate
683 in H⁺, Na⁺ and Ca²⁺ forms, *Colloids Surf.*, 24 (1987) 33-42.

- 684 [76] Y.-H. Li, Z. Di, J. Ding, D. Wu, Z. Luan, Y. Zhu, Adsorption thermodynamic, kinetic and
685 desorption studies of Pb²⁺ on carbon nanotubes, *Water Res.*, 39 (2005) 605-609.
- 686 [77] H. Gao, T. Kan, S. Zhao, Y. Qian, X. Cheng, W. Wu, X. Wang, L. Zheng, Removal of anionic
687 azo dyes from aqueous solution by functional ionic liquid cross-linked polymer, *J. Hazard. Mater.*,
688 261 (2013) 83-90.
- 689 [78] M. Ghaedi, B. Sadeghian, A.A. Pebdani, R. Sahraei, A. Daneshfar, C. Duran, Kinetics,
690 thermodynamics and equilibrium evaluation of direct yellow 12 removal by adsorption onto silver
691 nanoparticles loaded activated carbon, *Chem. Eng. J.*, 187 (2012) 133-141.
- 692 [79] C.-Y. Kuo, C.-H. Wu, J.-Y. Wu, Adsorption of direct dyes from aqueous solutions by carbon
693 nanotubes: Determination of equilibrium, kinetics and thermodynamics parameters, *J. Colloid
694 Interface Sci.*, 327 (2008) 308-315.
- 695 [80] R. Ahmad, R. Kumar, Adsorptive removal of congo red dye from aqueous solution using bael
696 shell carbon, *Appl. Surf. Sci.*, 257 (2010) 1628-1633.
- 697 [81] H. Kim, S.-O. Kang, S. Park, H.S. Park, Adsorption isotherms and kinetics of cationic and
698 anionic dyes on three-dimensional reduced graphene oxide macrostructure, *J. Ind. Eng. Chem.*, 21
699 (2015) 1191-1196.
- 700 [82] C.R. Minitha, M. Lalitha, Y.L. Jeyachandran, L. Senthilkumar, R.T. Rajendra Kumar,
701 Adsorption behaviour of reduced graphene oxide towards cationic and anionic dyes: Co-action of
702 electrostatic and $\pi - \pi$ interactions, *Mater. Chem. Phys.*, 194 (2017) 243-252.
703
704
705